Emergence of nontrivial low-energy Dirac fermions in antiferromagnet $EuCd_2As_2$

J.-Z. Ma†, H. Wang†, S.-M. Nie†,C-J.Yi†, Y.-F. Xu, H. Li, J. Jandke, W. Wulfhekel, Y.-B. Huang, D. West, P. Richard, A. Chikina, V. N. Strocov, J. Mesot, H.-M. Weng, S.-B. Zhang, Y.-G. Shi*, T. Qian*, M. Shi*, and H. Ding

Dr. J.-Z. Ma, Dr. J. Jandke, Dr. A. Chikina, Prof. V. N. Strocov, Prof. J. Mesot, Prof. M. Shi

Paul Scherrer Institute, Swiss Light Source

CH-5232 Villigen PSI, Switzerland

E-Mail: ming.shi@psi.ch

Dr. C-J. Yi, Dr. Y.-F. Xu, Dr. H. Li, Prof. P. Richard, Prof. H.-M. Wenig, Prof. Y.-G. Shi, Prof. T. Qian, Prof. H. Ding

Beijing National Laboratory for Condensed Matter Physics and Institute of Physics

Chinese Academy of Sciences

Beijing 100190, China

E-mail: ygshi@iphy.ac.cn, tqian@iphy.ac.cn

Dr. J.-Z. Ma, Prof. J. Mesot

Institute of Condensed Matter Physics, École Polytechnique Fédérale de Lausanne

CH-10 15 Lausanne, Switzerland

Dr. H. Wang, Dr. D. West, Prof. S.-B. Zhang

Department of Physics, Applied Physics, and Astronomy, Rensselaer Polytechnic Institute

This is the author manuscript accepted for publication and has undergone full peer review but has not been through the copyediting, typesetting, pagination and proofreading process, which may lead to differences between this version and the Version of Record. Please cite this article as doi: 10.1002/adma.201907565.

Troy, New York 12180, United States

Dr. S.-M. Nie

Department of Materials Science and Engineering, Stanford University

Stanford, CA 94305, United States

Dr. C.-J. Yi, Dr. Y.-F. Xu, Dr. H. Li, Prof. P. Richard, Prof. H. Ding

School of Physics, University of Chinese Academy of Sciences

Beijing 100190, China

Prof. W. Wulfhekel

Physikalisches Institut, Karlsruhe Institute of Technology
76131 Karlsruhe, Germany
Prof. Y.-B. Huang
Shanghai Synchrotron Radiation Facility, Shanghai Institute of Applied Physics

Chinese Academy of Sciences, Shanghai 201204, China

Prof. H.-M. Weng, Prof. Y.-G. Shi, Prof. T. Qian, Prof. H. Ding

Songshan Lake Materials Laboratory

Dongguan, Guangdong 523808, China

Prof. H. Ding

CAS Center for Excellence in Topological Quantum Computation, University of Chinese Academy of Sciences, Beijing 100190, China
Prof. P. Richard
Institut quantique, Université de Sherbrooke, 2500 boulevard de l'Université, Sherbrooke, Québec J1K 2R1, Canada

† These authors contributed to this work equally.

Parity-time symmetry plays an essential role for the formation of Dirac states in Dirac semimetals. So far, all of the experimentally identified topologically nontrivial DSMs possess both parity and time reversal symmetry. The realization of magnetic topological DSMs remains a major issue in topological material research. Here, combining angle resolved photoemission spectroscopy with density functional theory (DFT) calculations, it is ascertained that band inversion induces a topologically nontrivial ground state in $EuCd_2As_2$. As a result, ideal magnetic Dirac fermions with simplest double cone structure near the Fermi level emerge in the antiferromagnetic (AFM) phase. The magnetic order breaks time reversal symmetry, but preserves inversion symmetry. The double degeneracy of the Dirac bands is protected by a combination of inversion, time-reversal and an additional translation operation. Moreover, our calculations show that a deviation of the magnetic moments from the *c* axis leads to the breaking of C3 rotation symmetry, and thus, a small band gap opens at the Dirac point in the bulk. In this case, the system hosts a novel state containing axion insulator, AFM topological crystalline insulator and higher order topological insulator. Our results provide an enlarged platform for the quest of topological Dirac fermions in a magnetic system.

Topological Dirac semimetals (DSMs) host bulk quasiparticle excitations described by the Dirac equation near the Dirac points. They are formed by the crossing of two doubly degenerate bands, protected by the $\mathcal{PT}$ symmetry, where $\mathcal{P}$ is the inversion symmetry and $\mathcal{T}$ is the time reversal symmetry.[1-4] Usually, when $\mathcal{P}$ or $\mathcal{T}$ is broken, the double degeneracy is lifted

and a Dirac point splits into a pair or pairs of Weyl points with opposite chirality.[5-10] A theoretical analysis has shown that the DSM states can still survive in the magnetic system of CuMnAs, in which both $\mathcal{P}$ and $\mathcal{T}$ are broken, but the combined $\mathcal{PT}$ symmetry is preserved.[11] This prediction of nontrivial Dirac fermions still awaits experimental verification. In addition, further theoretical investigations proposed that Dirac fermions could also emerge from a system where either the $\mathcal{T}$ or $\mathcal{P}$ symmetry is preserved, but the $\mathcal{PT}$ symmetry is broken.[12-14] This indicates the significance of another symmetry operation which must be included when talking about the emergence of Dirac fermions. That is, the production of inversion $\mathcal{P}$, time-reversal $\mathcal{T}$ and an extra spatial symmetry operation, such as a translation or a rotation operation. This combined symmetry can protect the degeneracy of Dirac fermions and suggests that basic parity-time symmetry or each single symmetry is not an essential requirement for Dirac fermions. Whether nontrivial Dirac fermions can be realised in a system with only one of the $\mathcal{P}$ or $\mathcal{T}$ symmetries broken still awaits direct experimental verification.

A topological insulator (TI) hosts an insulator bulk state and conductive massless Dirac fermionic states at the surface, protected by the $\mathcal{T}$ symmetry. Usually, one would expect a lifting of this protection and an energy gap opening in the Dirac cone of surface states.[15] In case of a broken $\mathcal{T}$ symmetry, on the other hand, theoretical studies proposed that for some antiferromagnetic (AFM) systems, there are special surfaces, on which gapless surface Dirac cones are still protected by a combined $\mathcal{TL}$ symmetry,[14,16] the so-called nonsymmorphic time

reversal symmetry, where $\mathcal{L}$ is an additional crystalline symmetry operation, although the $\mathcal{T}$ symmetry is broken. Furthermore, it was shown that for other surfaces, there are gaped surface states contributing to half-quantized anomalous Hall conductivity. This class of AFM materials was coined as AFM TIs, and as a possible candidate for an axion insulator, as reported recently for $MnBi_2Te_4$.[17-21] However, the topological nature of the surface of $MnBi_2Te_4$ remains puzzling due to disagreements between experimental results and theoretical predictions.[19-21] Seeking new axion insulator candidates among magnetic topological materials remains a major issue in topological physics.

So far, two different A-type antiferromagnetic (AFM) orders have been suggested for the magnetic ground state of $EuCd_2As_2$,[22-24] i.e. one with spin along the in-plane direction[22] and one with spin along the out-of-plane direction.[23,24] Using density functional theory (DFT) calculations, we show that the DSM state can exist when the ground state of $EuCd_2As_2$ is in the out-of-plane spin configuration. In agreement with previous theoretical studies,[14] the Dirac crossing points are protected by the *C3* rotation symmetry around the *z* axis. The degeneracy of the Dirac bands is protected by the $\mathcal{PTL}$ symmetry operation that is the product of $\mathcal{PT}$ and $\mathcal{L}$, where $\mathcal{L}$ is a translation operator. The system is invariant under this operation. On the other hand, the in-plane A-type AFM spin configuration breaks the *C3* symmetry in the AFM state of $EuCd_2As_2$, which leads to a hybridization gap (~1 meV) and avoids the bands crossing along the k_z axis. As a consequence, the ground state of $EuCd_2As_2$ becomes a novel axion

insulator state which is not studied in previous theoretical paper.[14] This ground state is similar to that reported recently in the $MnBi_2Te_4$ family.[17,18] But for $EuCd_2As_2$, massless Dirac surface states appear on some specifically oriented surfaces which are protected by the mirror or $\mathcal{TL}$ symmetries. For other surfaces, which do not retain any mirror or $\mathcal{TL}$ symmetry, the surface states are gapped and the hinge states, associated with higher order TI states, emerge at the edges of these surfaces.[25,26] Although the spin fluctuation induced topology Weyl semimetal $EuCd_2As_2$ has been uncovered in the paramagnetic phase,[27] it still awaits to expose the variety of possible novel topological phases in the AFM ground states.

Using angle-resolved photoemission spectroscopy (ARPES), we show that in the AFM state of $EuCd_2As_2$ a band inversion takes place near the Fermi level (E_F), where the electronic structure has a double-cone structure. This observation is in good agreement with calculations. The ARPES results reveal that the bulk ground state of $EuCd_2As_2$ is a topologically nontrivial magnetic Dirac system, which is either an AFM DSM or an axion insulator. According to DFT calculations, the band gap which is associated with the breaking of the C_3 symmetry is around 1 meV. This is comparable to the thermal broadening effect at $\sim$ 3 K. Thus, it is impossible to clarify whether $EuCd_2As_2$ is an axion insulator or a DSM by using ARPES or another measurement technique carried out at relatively high temperature compared to the thermal broadening. Three-dimensional topological nontrivial magnetic DSM-like bands are expected to be observed in the ARPES spectra of $EuCd_2As_2$. The influence of spin directions on the electronic

structure is negligible compared to the thermal broadening effect for temperatures near or above 4.2 K (liquid Helium temperature).

$EuCd_2As_2$ has a layered structure with Cd_2As_2 layers separated by triangular Eu layers, as shown in Figure 1a. This structure belongs to the space group *P*-3*m*1 (no. 164). The Laue diffraction pattern of a $EuCd_2As_2$ single crystal shows a 6-fold rotation symmetry about the *c* axis (Figure 1d). The resistivity (Figure 1c) and the magnetic susceptibility χ (*T*) curves, with magnetic field (*H*) applied along the *c* axis (Figure 1e), exhibit a peak at 9.5 K. This indicates that the local Eu 4*f* moments form an AFM lattice at $T < 9.5$ K. The magnetization isotherms with *H* parallel to the *c* axis are plotted in Figure 1f for various temperatures. One can see that at low temperatures and under a 2 T magnetic field, the local moments of Eu^{2+} ions are almost fully polarized. The dashed line indicates the theoretical magnetic moment of free Eu^{2+} ions. Previous studies show that the anisotropy of the out-of-plane and in-plane resistivity dramatically increases below the Néel temperature (T_N). This implies that the Eu magnetic moments are ferromagnetically ordered within the *ab* plane and antiferromagnetically coupled along the *c* axis. This suggests that $EuCd_2As_2$ has the so-called *A*-type AFM structure on the Eu sites in the magnetically ordered state[23,24] (Figure 1a). In contrast to a peak occurring in the χ (*T*) curves for *H* along the *c* axis (Figure 1e), the χ (*T*) curve remains flat below T_N when *H* is parallel to the *ab* plane. This indicates that the ordered moments are along the *c* axis.[23,24,28-30] On the other

hand, a recent resonant elastic x-ray scattering (REXS) study suggests the same A-type antiferromagnetic structure, but with in-plane (ab-plane) magnetic moments.[22]

In the *A*-type AFM phase of $EuCd_2As_2$, the lattice constant *c* is doubled compared to the paramagnetic (PM) phase, as shown in Figure 1a. Because of the broken $\mathcal{T}$ symmetry and the conserved $\mathcal{P}$ symmetry in the magnetic unit cell (the inversion centre is marked as P_{AFM} in Figure 1a), the $\mathcal{PT}$ symmetry is broken. However, together with an additional translational operation $\mathcal{L}$, which corresponds to half the magnetic unit cell along the *c* axis (Figure 1a), the combined symmetry operation $\mathcal{PTL}$ makes the system invariant under transformation, with $(\mathcal{PTL})^2 = -1$. This results in a double degeneracy (Kramer's degeneracy) of all bands in the AFM phase of $EuCd_2As_2$, regardless of whether the magnetic moments are in-plane or out-of-plane.[14] Moreover, we can also choose the P_{PM} (centre of the PM unit cell, as shown in Figure 1a) as the inversion operation centre. In this case, the conduction $\mathcal{P}_{PM}\mathcal{T}$ symmetry is preserved and can also protect the double degeneracy of Dirac bands. This scenario is described in [11].

The symmetry above and below T_N plays an essential role for the band degeneracy and the detailed dispersion evolution, as well as for the topology of the band structure. The comparison of the band structure at 2K and 11K has been discussed in our previous study.[27] In addition to the two temperature points, in Figure 2 we show the ARPES spectra as a function of temperature, approaching and crossing T_N. The folded bands in the AFM phase are clearly observed, as shown in the black box (Figure 2f). But they disappear with increasing

temperature (Figure 2i). The continuous change of the band structure in Figure 2 indicates that ARPES detects the AFM phase transition, and that the band structure changes between the AFM and PM phases.

To explore the electronic structure in the AFM phase of $EuCd_2As_2$, we carried out DFT + U calculations with the Hubbard correction U on the Eu $4f$ orbitals (see section Methods for details). Firstly, we consider the A-type AFM order with out-of-plane magnetic moments. Figure 2c-j shows the energy bands along high-symmetry lines as a function of U. For U = 0, a number of flat bands composed by the Eu *4f* orbitals appear near E_F (Figure 3a). Upon increasing U, the Eu *4f* flat bands move downwards (Figure 3c-k) and are shifted to about 1 ~ 1.6 eV below E_F when U = 5 eV (Figure 3b).

Remarkably, our results reveal a band crossing on the Γ-A line when U > 3 eV. Around the Γ point, the band crossing arises from the band inversion of the energy bands with Cd 5s and As 4p orbital characters. These two bands are doubly degenerated and belong to different irreducible representations of the threefold rotation symmetry about the k_z axis. This prohibits the hybridization of these two bands and results in an unavoidable band crossing on the Γ-A line. The four-fold degeneracy of the crossing point occurs near E_F and is protected by the $\mathcal{PTL}$ symmetry. This implies that in the A-type AFM phase with out-of-plane magnetic moments, $EuCd_2As_2$ is a DSM. For the $k_z = 0$ plane, $(\mathcal{TL})^2 = -1$ and $\mathcal{TL} \cdot H(k_1, k_2, 0) \cdot (\mathcal{TL})^{-1} = H(-k_1, -k_2, 0)$, leading to the definition of the topological Z_2 index.[16] In the presence of the

inversion symmetry $\mathcal{P}$, the Z_2 index can be further simplified as follows $(-1)^{Z_2} = \prod_{i=1}^{4} \prod_{n=1}^{n_{occ}/2} \xi_{2n}(K_i)$, where $K_1$is the Γ point and $K_{2,3,4}$ are the three M points. $\xi_{2n}(K_i)$ is the parity eigenvalue of the 2n-th band at the K_i point. n_{occ} is the total number of the occupied bands. Based on the parity information in Table 1, we found out Z_2=1 for the k_z = 0 plane, associated with the band inversion, and Z_2 = 0 at k_z = π plane, illustrating the nontrivial band topology of the DSM state[31,32] in $EuCd_2As_2$. From the calculated band structure in Figure 3c-j, we construct a topological phase diagram of $EuCd_2As_2$ as a function of *U* (Figure 3l). The band topology in the AFM phase is closely related to the correlation strength of the Eu *4f* states. As *U* increases from 0 to 8 eV, a phase transition from a heavy fermion trivial semimetal state, without band inversion, to an ideal DSM state takes place around *U* = 3 eV.

Table 1: The number of occupied bands with even and odd parity at the eight time-reversal-invariant moment (TRIM). The number of the occupied bands is 38.

TRIM	+	-
Γ	14	24
3M	12	26
A	19	19
3L	19	19

To justify the theoretical prediction that $EuCd_2As_2$ is a nontrivial Dirac material in the AFM phase, the first necessary step is to experimentally determine the location of the Eu *4f*

states, in order to confirm that the position of Eu *4f* states agrees with the calculations with $U > 3$ eV. Figure 2 shows that the experimental Eu 4*f* states locate in an energy range about 1 ~ 1.6 eV below E_F. The calculated positions of the Eu *4f* states with $U = 5$ eV, as well as the band dispersions near E_F, are consistent with our ARPES measurements, as presented in Figure 2 and Figure 5. This indicates that the real material $EuCd_2As_2$ locates in the topological DSM region, if the magnetic moments are parallel or antiparallel to the *c* axis. Another important property of a topological DSM are the surface Fermi arc states. For checking the nontrivial topological nature of the DSM state in $EuCd_2As_2$, we calculated the surface states on the nature cleavage (101) projection (Figure 3m,n). Surface Fermi arcs connecting the Dirac points are observed. These surface states are located in a very small energy and momentum region which makes it nearly impossible to be measured by ARPES. Moreover, without the $\mathcal{TL}$ symmetry protection, the surface states are gapped (Fig. 3n) which is different to the normal DSM. On the other hand, the surface sates on (001) or (010) surfaces are protected by $\mathcal{TL}$ symmetry.[14]

Subsequently, we performed band structure calculations for the A-type AFM ordered phase with in-plane magnetic moments. In this case, the C_3 symmetry is broken. The general band structure is very similar to that of the out-of-plane AFM order, except for a gap (~ 1 meV) opening at the bulk Dirac cone point. As a result, the system evolves into an AFM topological (crystalline) insulator with a massive bulk Dirac cone as shown in Figure 4a,b. Due to the

presence of a band gap in the bulk and the preserved $\mathcal{P}$ symmetry, it is possible to calculate the topological parity-based invariant Z_4 index, which is defined as $Z_4 = \sum_{i=1}^{8} \sum_{n=1}^{n_{occ}} \frac{1+\xi_n(K_i)}{2}$ mod 4.[33] From the calculated band structure of $EuCd_2As_2$, we obtained Z_4 = 2. It is known that for an axion insulator, the quantized number θ is described by the Z_2 index, and when inversion symmetry is preserved and time reversal symmetry is broken, the quantized number θ can be reduced to the Z_4 index [25,34,35]. A nonzero Z_4 = 2 index is associated with the nontrivial axion insulator state[25] which appears in $EuCd_2As_2$. Because $EuCd_2As_2$ has two natural cleavage surfaces,[27] i.e. the (001) and (101) surface, it is relevant to calculate the surface states at these surfaces. Protected by the mirror symmetry (M_x), spins align along the *x* direction (Figure 4c) and massless Dirac surface states can occur at the (001) surface. But the Dirac point does not locate at any high-symmetry point (Figure 4d-f). The calculated result is consistent with the STS/STM data acquired on (001) surface, which shows no signature of a gap opening at 4.2K (Figure 5e), indicating that there is no experimental visible gap on the (001) surface, as predicted and discussed by the calculation results above 3K. On the other hand, as both the mirror and $\mathcal{TL}$ symmetries are broken on the (101) surface, the surface states are gapped (Figure 4g-i). Furthermore, because of the nonzero Z_4 index in the bulk, hinge modes are expected to emerge on these special edges which are protected by the inversion symmetry in case the surface states are gapped.[25,26,35] Thus, in case of an existing in-plane spin configuration

of the AFM ground state, $EuCd_2As_2$ would be a candidate for higher order TI with a hinge state on the edges between specific surface orientations.

In order to explore its topological properties, we systematically studied the electronic structure of $EuCd_2As_2$ by using high resolution ARPES. Figure 5 shows the experimentally determined band dispersions in the bulk BZ. A 3D Dirac cone structure is unveiled at temperatures below T_N. An important aspect for verifying the theoretical prediction is to identify the "M" shape like double-cone crossing points along the Γ-A line and a cone-shaped dispersion in the k_x-k_y plane (Figure 5c,h). These signatures would be a fingerprint of the Dirac state in the AFM phase of $EuCd_2As_2$.

The ARPES data in Figure 5a-g were acquired from a cleaved (001) surface. Figure 5a shows a wide band structure acquired at 5K with $h\nu$ = 70 eV that defines a cut in momentum space crossing the Dirac point (Figure 5d,e), with good agreement with the LDA calculations (Figure 5a). The 3D ARPES intensity plot in Figure 5b shows that near E_F the bands disperse nearly isotropically in the k_x-k_y plane. Figure 5f,g exhibits several hole-like bands along the Γ-K and Γ-M directions. We assign the outmost hole-like bands to be the lower branch of the Dirac cone in the k_x-k_y plane. The hole-like bands cross E_F at a Fermi wave vector of ~ 0.1 $Å^{-1}$, intersect above E_F and form a small circular FS at the BZ centre, as shown in Figure 5e.

In order to achieve high momentum resolution along the Γ-A direction and in order to minimize the effect of the intrinsic broadening of the momentum component perpendicular to the sample surface, we carried out ARPES measurements on a cleaved (101) surface instead of a (001) surface. With respect to this surface, the Γ-A line has a large in-plane component that is conserved in the photoemission process. Figure 5j shows the band dispersions acquired with $h\nu$ = 90 eV, which corresponds to a momentum cut passing through the Γ point and approximately along the Γ-A line, as indicated in the FS map in Figure 5i. We observe two bands crossing at ±0.05 $Å^{-1}$, close to the Γ point. This is consistent with the Dirac points from our band calculations, as shown in Figure 5k. Furthermore, the "M" shape band structure along the Γ-A line indicates that there is an inversion between the Cd *5s* and As *4p* bands. Since both the DSM state and the Z_4 index are associated with band inversion, the observation of an "M" shaped dispersion provides compelling evidence to the theoretical prediction that $EuCd_2As_2$ is a magnetic nontrivial topological material, regardless of whether a band gap occurs at the "Dirac point" and whether it can be resolved at finite temperature and with finite energy resolution. When increase temperature above the T_N, the band structure along Γ-A line agree well with the FM model calculation rather than AFM DSM states induced by strong FM spin fluctuations. [27]

We note that the energy positions of the hole-like band top on the (101) and (001) surfaces are different. The result is repeatable in our experiments and could be caused by surface potentials, which result in a bending of the energy bands for some cleaved surfaces.[36,37]

Because the Dirac points locate almost at E_F, the upper branch of the Dirac cone is unoccupied and cannot be probed by ARPES. However, STM/STS is a good method to detect the upper branch. Our STM/STS data recorded at 4.2K (inset of Figure 5j and Figure 5l) shows a "V" shape spectrum near E_F, indicating that, there is a Dirac cone band structure and no sign of a gap (> 4.2 K) in the density of states.

Theoretically, the coexistence of Dirac fermions and local magnetic moments in this system provides a platform for studying the Kondo effect and the RKKY interaction in Dirac materials. In Figure 1c, the resistivity at zero field exhibits a Kondo-like shape above T_N, suggesting that the carriers are strongly scattered by the local magnetic moments of Eu. While the Kondo effect and the RKKY interaction in DSMs and WSMs have been studied theoretically,[38-42] our results suggest that $EuCd_2As_2$ can be a platform to study them experimentally.

The observation of the "M" shape spectra and the lineally dispersive double-cone structure near E_F indicates the existence of ideal nontrivial states induced by band inversion. Using ARPES combined with DFT calculations, we have shown that $EuCd_2As_2$ is a magnetic nontrivial clean topological Dirac material in the AFM phase in which the $\mathcal{T}$ symmetry is broken. On the other hand, the double degeneracy of the energy bands is protected by the $\mathcal{PTL}$ symmetry, with broken $\mathcal{T}$ symmetry. Magnetic DSMs are reported in the AFM FeSn and $CaMnBi_2$ families as well.[43,44] However, these materials obey trivial band structure without topological properties. For FeSn, the electronic structure is topologically trivial and the Dirac points are the highly

degenerated points according to the symmetries of the space group. These points cannot be associated with any nonzero topological invariant and don't lead to protected topological surface states. For the $CaMnBi_2$ family, the Dirac points disappear when SOC is taken into account. Thus, $EuCd_2As_2$ is the first experimentally realised magnetic topological DSM. Moreover, the STS data shows a "V" shape density of states near E_F without visible gap at 4.2 K. The agreement between the experimental results and the calculations suggests that $EuCd_2As_2$ is a good AFM DSM or axion insulator candidate, as well as a higher order TI at extreme low temperatures. $EuCd_2As_2$ shows many unique properties, such as the coexistence of Dirac fermions and local magnetic moments, as well as a metamagnetic transition under moderate magnetic fields. $EuCd_2As_2$ is a promising platform to explore exotic physical phenomena related to Dirac fermions in magnetic systems.

Experimental Section

Single crystals of $EuCd_2As_2$ were synthesized using Sn as flux. Starting materials of Eu (ingot, 99.9%, Alfa Aesar), Cd (grain 99.999%, Alfa Aesar), As (ingot, 99.999%, Alfa Aesar) and excess Sn (grain 99.9969%, Alfa Aesar) were mixed and loaded in an alumina crucible at a molar ratio of 1:2:2:10. The operations were performed in a glove box filled with pure argon. Then the crucible was sealed in a quartz tube under high vacuum. The tube was heated to 900°C and maintained for 20 hours before being slowly cooled to 500°C at a rate of 2°C /hour. Then, the samples were separated from the Sn in a centrifuge.

ARPES measurements were performed at the "Dreamline" beamline of the Shanghai Synchrotron Radiation Facility (SSRF) with a Scienta DA30 analyser, SIS-HRPES beam line with a Scienta R4000 analyser and ADRESS beamline with a SPECS analyser of the Swiss Light Source (PSI), beamline I05 in Diamond Light Source of UK, and beamline UE112 PGM-2b-1^3 at BESSY Synchrotron. The energy and angular resolutions were set to 5~30 meV and 0.2°, respectively. The samples for ARPES measurements were cleaved *in situ* and measured in a temperature range between 2.5 K and 30 K and in a vacuum better than 5×10^{-11} Torr. STM measurements were carried out by using a home-built Joule-Thomson STM (JT-STM).[45] The $EuCd_2As_2$ single crystals were cleaved in situ at T = 77 K. Measurements were performed at T = 2.8 - 14 K.

The calculations based on density functional theory (DFT) were performed using VASP.[46,47] The interaction between ion cores and valence electrons is described by the projector-augmented wave (PAW) method. The Perdew-Burke-Ernzerhof (PBE) approximation[48] was used for the exchange-correlation function. Plane waves with a kinetic energy cutoff of 500 eV were used as basis set. A Γ-centred *k*-point mesh with a sufficient k-point density was used to sample the bulk BZ. The total energy convergence criterion was set to be 10^{-7} eV. The atomic structures were optimized until the Hellman-Feynman forces were smaller than 0.2 mRy/Bohr. Spin-orbit coupling was implemented in the all-electron part of the PAW Hamiltonian within the muffin-tin spheres. DFT + U correction was applied to the Eu 4*f* orbits.

Acknowledgements

We acknowledge E. Rienks, Timur K. Kim, L.-Y. Kong, Y.-G. Zhong, and H.-J. Liu for the assistance during the measurements. We acknowledge T. Shang for useful discussions. This work was supported by the Ministry of Science and Technology of China (2016YFA0300600, 2016YFA0401000, and 2017YFA0302901), the National Natural Science Foundation of China (11622435, 11474340, 11474330, 11674369, and 11422428), the Sino-Swiss Science and Technology Cooperation (Grant No. IZLCZ2-170075), the NCCR-MARVEL funded by the Swiss National Science Foundation, the Swiss National Science Foundation (No. 200021_182695), the Chinese Academy of Sciences (XDB07000000 and QYZDB-SSW-SLH043), and Beijing Municipal Science & Technology Commission (No. Z171100002017018). Y.-B.H. acknowledges funding from the CAS Pioneer Hundred Talents Program (type C). S.-B.Z. and H.W. was supported by the US Department of Energy (DOE) under Grant No. DESC0002623. This work used the Extreme Science and Engineering Discovery Environment (XSEDE), which is supported by National Science Foundation grant number ACI-1548562. S.-B.Z. acknowledges computational resources from Stampede supercomputer at TACC made available by XSEDE through allocation TG-DMR180114. This research was undertaken thanks in part to funding from the Canada First Research Excellence Fund.

Keywords

Condensed Matter Physics, magnetic Dirac semimetal, axion insulator, higher order topological insulator.

References:

[1] Z. Wang, Y. Sun, X.-Q. Chen, C. Franchini, G. Xu, H. Weng, X. Dai, Z. Fang, *Phys. Rev. B* **2012**, *85*, 195320.

[2] Z. K. Liu, B. Zhou, Y. Zhang, Z. J. Wang, H. M. Weng, D. Prabhakaran, S.-K. Mo, Z. X. Shen, Z. Fang, X. Dai, Z. Hussain, Y. L. Chen, *Science* **2014**, *343*, 864.

[3] Z. Wang, H. Weng, Q. Wu, X. Dai, Z. Fang, *Phys. Rev. B* **2013**, *88*, 125427.

[4] Z. K. Liu, J. Jiang, B. Zhou, Z. J. Wang, Y. Zhang, H. M. Weng, D. Prabhakaran, S.-K. Mo, H. Peng, P. Dudin, T. Kim, M. Hoesch, Z. Fang, X. Dai, Z. X. Shen, D. L. Feng, Z. Hussain, Y. L. Chen, *Nat. Mater.* **2014**, *13*, 677.

[5] H. Weng, C. Fang, Z. Fang, B. A. Bernevig, X. Dai, *Phys. Rev. X* **2015**, *5*, 11029.

[6] S.-M. Huang, S.-Y. Xu, I. Belopolski, C.-C. Lee, G. Chang, B. Wang, N. Alidoust, G. Bian, M. Neupane, C. Zhang, S. Jia, A. Bansil, H. Lin, M. Z. Hasan, *Nat. Commun.* **2015**, *6*, 7373.

[7] B. Q. Lv, H. M. Weng, B. B. Fu, X. P. Wang, H. Miao, J. Ma, P. Richard, X. C. Huang, L. X. Zhao, G. F. Chen, Z. Fang, X. Dai, T. Qian, H. Ding, *Phys. Rev. X* **2015**, *5*, 31013.

[8] S.-Y. Xu, I. Belopolski, N. Alidoust, M. Neupane, G. Bian, C. Zhang, R. Sankar, G. Chang, Z. Yuan, C.-C. Lee, S.-M. Huang, H. Zheng, J. Ma, D. S. Sanchez, B. Wang, A. Bansil, F. Chou, P. P. Shibayev, H. Lin, S. Jia, M. Z. Hasan, *Science* **2015**, *349*, 613 LP.

[9] B. Q. Lv, N. Xu, H. M. Weng, J. Z. Ma, P. Richard, X. C. Huang, L. X. Zhao, G. F. Chen, C. E. Matt, F. Bisti, V. N. Strocov, J. Mesot, Z. Fang, X. Dai, T. Qian, M. Shi, H. Ding, *Nat. Phys.* **2015**, *11*, 724.

[10] S. Nie, G. Xu, F. B. Prinz, S. Zhang, *Proc. Natl. Acad. Sci.* **2017**, *114*, 10596 LP.

[11] P. Tang, Q. Zhou, G. Xu, S.-C. Zhang, *Nat. Phys.* **2016**, *12*, 1100.

[12] S. Ok, M. Legner, T. Neupert, A. M. Cook, *arXiv:1703.03804v4*, **2017**.

[13] H. Gao, Y. Kim, J. W. F. Venderbos, C. L. Kane, E. J. Mele, A. M. Rappe, W. Ren, *Phys. Rev. Lett.* **2018**, *121*, 106404.

[14] G. Hua, S. Nie, Z. Song, R. Yu, G. Xu, K. Yao, *Phys. Rev. B* **2018**, *98*, 201116.

[15] Y. L. Chen, J.-H. Chu, J. G. Analytis, Z. K. Liu, K. Igarashi, H.-H. Kuo, X. L. Qi, S. K. Mo, R. G. Moore, D. H. Lu, M. Hashimoto, T. Sasagawa, S. C. Zhang, I. R. Fisher, Z. Hussain, Z. X. Shen, *Science* **2010**, *329*, 659 LP.

[16] R. S. K. Mong, A. M. Essin, J. E. Moore, *Phys. Rev. B* **2010**, *81*, 245209.

[17] J. Li, Y. Li, S. Du, Z. Wang, B.-L. Gu, S.-C. Zhang, K. He, W. Duan, Y. Xu, *Sci. Adv.* **2019**, *5*, eaaw5685.

[18] D. Zhang, M. Shi, T. Zhu, D. Xing, H. Zhang, J. Wang, *Phys. Rev. Lett.* **2019**, *122*, 206401.

[19] Y.-J. Hao, P. Liu, Y. Feng, X.-M. Ma, E. F. Schwier, M. Arita, S. Kumar, C. Hu, R. Lu, M. Zeng, Y. Wang, Z. Hao, H.-Y. Sun, K. Zhang, J. Mei, N. Ni, L. Wu, K. Shimada, C. Chen, Q. Liu, C. Liu, *Phys. Rev. X* **2019**, *9*, 41038.

[20] H. Li, S.-Y. Gao, S.-F. Duan, Y.-F. Xu, K.-J. Zhu, S.-J. Tian, J.-C. Gao, W.-H. Fan, Z.-C. Rao, J.-R. Huang, J.-J. Li, D.-Y. Yan, Z.-T. Liu, W.-L. Liu, Y.-B. Huang, Y.-L. Li, Y. Liu, G.-B. Zhang, P. Zhang, T. Kondo, S. Shin, H.-C. Lei, Y.-G. Shi, W.-T. Zhang, H.-M. Weng, T. Qian, H. Ding, *Phys. Rev. X* **2019**, *9*, 41039.

[21] Y. J. Chen, L. X. Xu, J. H. Li, Y. W. Li, H. Y. Wang, C. F. Zhang, H. Li, Y. Wu, A. J. Liang, C. Chen, S. W. Jung, C. Cacho, Y. H. Mao, S. Liu, M. X. Wang, Y. F. Guo, Y. Xu, Z. K. Liu, L. X. Yang, Y. L. Chen, *Phys. Rev. X* **2019**, *9*, 41040.

[22] M. C. Rahn, J.-R. Soh, S. Francoual, L. S. I. Veiga, J. Strempfer, J. Mardegan, D. Y. Yan, Y. F.

Guo, Y. G. Shi, A. T. Boothroyd, *Phys. Rev. B* **2018**, *97*, 214422.

[23] H. P. Wang, D. S. Wu, Y. G. Shi, N. L. Wang, *Phys. Rev. B* **2016**, *94*, 45112.

[24] I. Schellenberg, U. Pfannenschmidt, M. Eul, C. Schwickert, R. Pöttgen, *Zeitschrift für Anorg. und Allg. Chemie* **2011**, *637*, 1863.

[25] Y. Xu, Z. Song, Z. Wang, H. Weng, X. Dai, *Phys. Rev. Lett.* **2019**, *122*, 256402.

[26] F. Schindler, A. M. Cook, M. G. Vergniory, Z. Wang, S. S. P. Parkin, B. A. Bernevig, T. Neupert, *Sci. Adv.* **2018**, *4*, eaat0346.

[27] J.-Z. Ma, S. M. Nie, C. J. Yi, J. Jandke, T. Shang, M. Y. Yao, M. Naamneh, L. Q. Yan, Y. Sun, A. Chikina, V. N. Strocov, M. Medarde, M. Song, Y.-M. Xiong, G. Xu, W. Wulfhekel, J. Mesot, M. Reticcioli, C. Franchini, C. Mudry, M. Müller, Y. G. Shi, T. Qian, H. Ding, M. Shi, *Sci. Adv.* **2019**, *5*, eaaw4718.

[28] N. D. Ashcroft, N.W. and Mermin, *Solid State Phys.*, Holt, Rinehart And Winston, **1976**, pp. 702–709.

[29] D. G. Quirinale, V. K. Anand, M. G. Kim, A. Pandey, A. Huq, P. W. Stephens, T. W. Heitmann, A. Kreyssig, R. J. McQueeney, D. C. Johnston, A. I. Goldman, *Phys. Rev. B* **2013**, *88*, 174420.

[30] S. Jiang, Y. Luo, Z. Ren, Z. Zhu, C. Wang, X. Xu, Q. Tao, G. Cao, Z. Xu, *New J. Phys.* **2009**, *11*, 25007.

[31] C. L. Kane, E. J. Mele, *Phys. Rev. Lett.* **2005**, *95*, 146802.

[32] L. Fu, C. L. Kane, E. J. Mele, *Phys. Rev. Lett.* **2007**, *98*, 106803.

[33] H. C. Po, A. Vishwanath, H. Watanabe, *Nat. Commun.* **2017**, *8*, 50.

[34] E. Khalaf, H. C. Po, A. Vishwanath, H. Watanabe, *Phys. Rev. X* **2018**, *8*, 31070.

[35] E. Khalaf, *Phys. Rev. B* **2018**, *97*, 205136.

[36] H.-J. Noh, H. Koh, S.-J. Oh, J.-H. Park, H.-D. Kim, J. D. Rameau, T. Valla, T. E. Kidd, P. D. Johnson, Y. Hu, Q. Li, *Europhys. Lett.* **2008**, *81*, 57006.

[37] M. Bianchi, D. Guan, S. Bao, J. Mi, B. B. Iversen, P. D. C. King, P. Hofmann, *Nat. Commun.* **2010**, *1*, 128.

[38] M. V. Hosseini, M. Askari, *Phys. Rev. B* **2015**, *92*, 224435.

[39] A. K. Mitchell, L. Fritz, *Phys. Rev. B* **2015**, *92*, 121109.

[40] H.-R. Chang, J. Zhou, S.-X. Wang, W.-Y. Shan, D. Xiao, *Phys. Rev. B* **2015**, *92*, 241103.

[41] Y. Sun, A. Wang, *J. Phys. Condens. Matter* **2017**, *29*, 435306.

[42] H.-H. Lai, S. E. Grefe, S. Paschen, Q. Si, *Proc. Natl. Acad. Sci.* **2018**, *115*, 93 LP.

[43] Z. Lin, C. Wang, P. Wang, S. Yi, L. Li, Q. Zhang, Y. Wang, Z. Wang, Y. Sun, Z. Sun, others, *arXiv:1906.05755*, **2019**.

[44] J. Park, G. Lee, F. Wolff-Fabris, Y. Y. Koh, M. J. Eom, Y. K. Kim, M. A. Farhan, Y. J. Jo, C. Kim, J. H. Shim, J. S. Kim, *Phys. Rev. Lett.* **2011**, *107*, 126402.

[45] L. Zhang, T. Miyamachi, T. Tomanić, R. Dehm, W. Wulfhekel, *Rev. Sci. Instrum.* **2011**, *82*, 103702.

[46] G. Kresse, J. Furthmiiller, *Comput. Mater. Sci.* **1996**, *6*, 15.

[47] G. Kresse, J. Furthmüller, *Phys. Rev. B* **1996**, *54*, 11169.

[48] J. P. Perdew, K. Burke, M. Ernzerhof, *Phys. Rev. Lett.* **1996**, *77*, 3865.

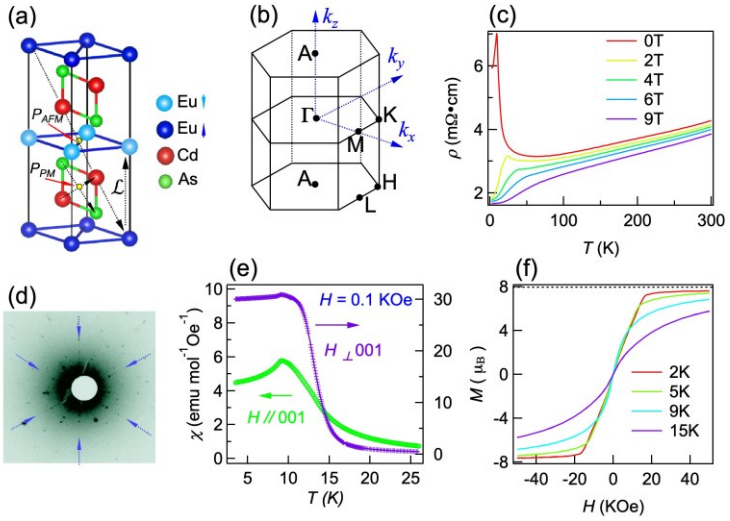

Figure 1. Crystal structure and basic physical properties of $EuCd_2As_2$. a) Crystal structure of $EuCd_2As_2$. The two colours of Eu atoms indicate two different spin alignments. b) 3D bulk BZ with high-symmetry points and coordinate axes. c) Temperature-dependent resistivity curves at different magnetic fields. d) Laue diffraction pattern of $EuCd_2As_2$ single crystal showing 6-fold rotation symmetry of the crystal structure about the *c* axis. e) Magnetic susceptibility curves with *H* parallel and perpendicular to the *c* axis, respectively. f) Magnetization isotherms with *H* parallel to the *c* axis at various temperatures. The dashed line indicates the theoretical magnetic moment for free Eu^{2+} ions.

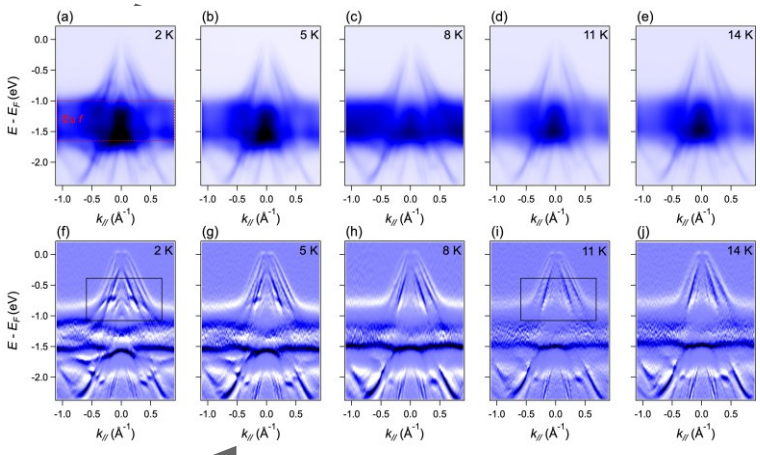

Figure 2. Temperature evolution of the band structure of $EuCd_2As_2$ across T_N = 9.5 K. a-e) Band structure along the cut indicated in Fig. 4(i) recorded at different temperatures below and above T_N. The red box shows the energy location of Eu 4*f* orbital states. f-j) Related curvature intensity plots. The black boxes show the folded bands at AFM phase that disappear with temperature increasing.

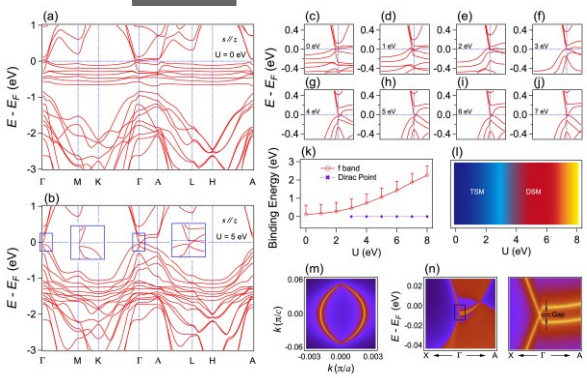

Figure 3. Calculated band structure of $EuCd_2As_2$ in the AFM phase with the out-of-plane spin configuration. a,b) Band structure along high-symmetry lines with the spin aligned along the *z* direction and U = 0 and 5 eV, respectively. The blue inset boxes show details of the bands near E_F, with a gapless Dirac-like band crossing on the Γ-A line. c-j) Band structure along K-Γ-A with the spin along the *z* direction and U varied from 0 to 7 eV. k) Binding energies of the topmost Eu *4f* flat band and Dirac point as a function of U. l) Phase diagram of $EuCd_2As_2$ in the AFM phase for U changing from 0 to 8 eV. TSM: Trivial Semimetal. m) Calculated Fermi arcs connecting two Dirac points projected to (101) surface. n) Band structure calculations projection to (101) surface and the zoomed in view.

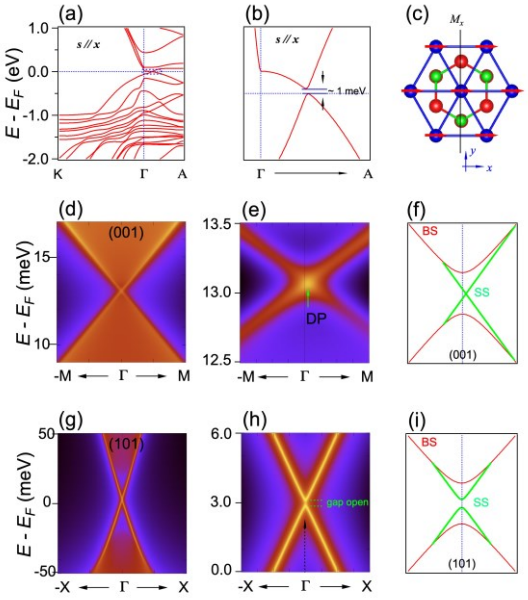

Figure 4. Calculated band structures of $EuCd_2As_2$ in the AFM phase with the in-plane spin configuration. a) Band structure along K-Γ-A with the spin aligned along the *y* direction and U = 5 eV. b) Zoom-in view of the blue box in a, indicating the gapped massive Dirac cone structure. c) M_x mirror symmetry shown in the crystal structure with spins along the *x* direction. d) Dirac cone surface state along the $k_y = 0$ path of the (001) surface protected by M_x. e) Zoom-in view of (d). The arrow shows that the Dirac point does not locate at the Γ point. f) Schematic diagram of topological surface states in d and e. g) Surface state along the $k_y = 0$ path of the (101) surface. h) Zoom-in view of (g). In absence of mirror symmetry protection, a small gap opens at the crossing point. i) Schematic diagram of topological surface states in (g) and (h).

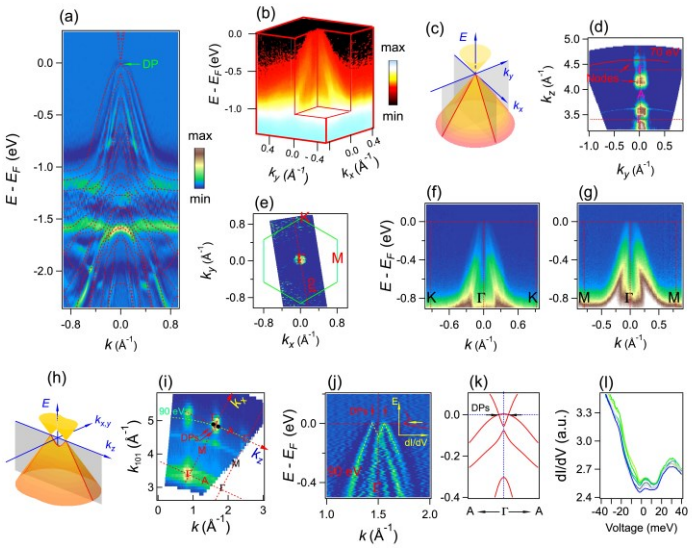

Figure 5. Band structure of 3D Dirac cones in $EuCd_2As_2$. a) Curvature intensity plot of the band structure along the cut noted in (e) recorded at 5 K, with the calculated bands superimposed. b) 3D ARPES intensity plot near E_F in the k_x-k_y plane at 70 eV and 6.5 K. c) Schematic of the 3D Dirac cone band structure in the k_x-k_y plane. d) Photon-energy-dependent ARPES intensity map at E_F, acquired from the cleaved (001) surface, indicating Fermi surface nodes along the k_z-k_y plane. e) FS intensity map extracted from (b). f,g) ARPES intensity plots recorded at 6.5 K along K-Γ-K and M-Γ-M, respectively. h) Schematic of the 3D Dirac cone band structure in the k_x-k_z plane at k_y = 0. Two Dirac points are located along the Γ-A line. The red curve indicates the occupied branch of Dirac bands. i) ARPES intensity map at E_F, acquired from the cleaved (101) surface with $h\nu$ varying from 30 to 120 eV at 20 K. j) Curvature intensity plot of the data acquired on the (101) surface with $h\nu$ = 90 eV at 6.5 K. The momentum location of the cut, indicated in (i), is nearly along Γ–A. The STS data near the Fermi level, shown in inset, show a "V" shape density of states without any visible gap opening. k) Calculated band structure along A-Γ–A. l) Differential tunnelling conductance spectra (I = -354 pA, U = -90 mV), recorded at various spatial positions at T = 4.2K.

When magnetism meets topology, colorful novel states can be created in materials. The realization of magnetic topological Dirac materials remains a major issue in the topological physics study. In this work, it is ascertained that the topologically nontrivial ground state of $EuCd_2As_2$ is a good candidate for magnetic topological DSM, axion insulator, AFM TCI, and higher order TI.